3-2005

Empirical Analysis of Aerial Camera Filters for Shoreline Mapping

Christopher Parrish
University of New Hampshire, Durham

Maryellen Sault
NOAA

Stephen A. White
University of New Hampshire, Durham

Jon Sellars
NOAA

EMPIRICAL ANALYSIS OF AERIAL CAMERA FILTERS FOR SHORELINE MAPPING

Christopher E. Parrish, Physical Scientist
Maryellen Sault, Cartographer
Stephen A. White, Research Engineer
Jon Sellars, Research Engineer
NOAA, NOS, National Geodetic Survey
Remote Sensing Division
1315 East-West Highway
Silver Spring, MD 20910
Chris.Parrish@noaa.gov
Maryellen.Sault@noaa.gov
Stephen.A.White@noaa.gov
Jon.Sellars@noaa.gov

ABSTRACT

Accurate, up-to-date national shoreline is critical in defining the territorial limits of the Unites States, updating nautical charts, and managing coastal resources. The National Oceanic and Atmospheric Administration (NOAA) delineates the interpreted shoreline photogrammetrically using tide-coordinated stereo photography acquired with black-and-white infrared emulsion. In this paper, we present the results of a two-phased study aimed at quantifying the effect of camera filter selection on the interpreted shoreline when utilizing this method of shoreline mapping.

INTRODUCTION

The National Oceanic and Atmospheric Administration (NOAA) is congressionally mandated to map the national shoreline. The primary method of shoreline mapping used at NOAA is through tide-coordinated stereo photography (Graham et al., 2003). Black-and-white infrared (B&WIR) emulsion is advantageous in this application because infrared radiation is strongly absorbed by water. Therefore, by using a long wavepass camera filter (Figure 1) to block wavelengths below a specified cut-on in the near infrared, areas of water can be made to appear black in the photography (Keller, 1974; Sabins, 1987). This greatly facilitates determination of the land/water interface.

The transmittance of very near infrared light just outside the visible portion of the electromagnetic spectrum is relatively high in seawater. Hence, selection of an appropriate filter is necessary to provide strong contrast between land and water in the photography and to ensure that shallow water areas are not misinterpreted as land. Based on research conducted in the late 1960s and early 1970s, NOAA recommends use of a 740 nm filter for shoreline B&WIR photography (Smith, 1978; Simmons, W., 2001, personal correspondence). However, due to the high cost of 740 nm filters, photography acquisition contractors are currently utilizing less expensive (and more readily available) 700 or 705 nm filters.

Our objective in this study was to examine and quantify the effect of filter selection through a two-phased experiment. In the first phase, two cameras, one fitted with a 705 nm filter and the other with a 740 nm filter, were used to acquire shoreline photography simultaneously. Experienced photogrammetrists then delineated the land/water interface from each set of photography in a softcopy photogrammetry environment. The compiled land/water interface vectors were then compared against GPS ground truth. In the second phase, CASI 2 hyperspectral imagery was used to simulate film photography with a variety of different filters. Results from both phases indicate that in areas of shallow water over bright sandy bottom, use of a 740 nm filter facilitates delineation of a consistent, accurate shoreline, especially with less experienced compilers.

Figure 1. Left: Long wavepass filter for B&WIR photography. Right: Installing the filter on the Wild RC30 lens cone.

PHASE 1

Background

Two camera filters were acquired for use in the first phase of this experiment: a NOAA-owned 740 nm filter and a 705 nm filter rented from I.K. Curtis, Inc. (Burbank, California). Prior to acquisition of aerial photography, the optical properties of the filters were tested at the National Institute of Standards and Technology (NIST). Figure 2 shows the transmittance spectra obtained from NIST for the two filters, along with the transmittance spectrum of pure seawater. The seawater transmittance spectrum was calculated from diffuse attenuation coefficients given in Smith and Baker (1981) and the following form of the Lambert-Beer Law:

$$T \{ \ e^{3\,Kd} \tag{1}$$

In Equation 1, K is the diffuse attenuation coefficient and d is the depth, which we have arbitrarily taken to be 1 m.

The graphs in Figure 2 indicate that the 705 nm filter was manufactured closer to its design specifications than the 740 nm filter. Long wavepass filters are characterized by the cut-on wavelength (i.e., the wavelength below which radiation is blocked and above which it is transmitted). Leica Geosystems, AG (formerly Wild), the manufacturer of the two filters used in this study, defines the cut-on wavelength as the point of 50% of peak transmittance (Leica, 2003). Using this definition, the cut-on wavelength for the 740 nm filter is actually 725 nm, while the cut-on for the 705 nm filter is actually 702 nm.

According to Leica Geosystems, the deviation between the nominal and actual cut-on wavelengths is easily explained through analysis of the manufacturing process (Zuberbuehler, F., 2004, personal correspondence). Because high geometric accuracy is typically the most important criterion in photogrammetric applications, the filter manufacturer must concentrate most heavily on ensuring a high degree of parallelism of the filter surfaces and avoiding local variation due to non-uniform melting of the glass. The fine polishing necessary to meet the geometric accuracy specifications will cause some deviation in the cut-on wavelength.

Despite the apparent differences in the manufacture of the two filters, the graphs in Figure 2 nicely illustrate the theory behind selection of the 740 nm filter. The transmittance of light in seawater drops off most sharply (i.e., has the steepest slope) between 700 and 730 nm. Hence, the 740 nm filter should do a better job of blocking wavelengths with higher transmittance in water, thereby providing sharper contrast between land and water and ensuring that shallow water areas are not misinterpreted as land.

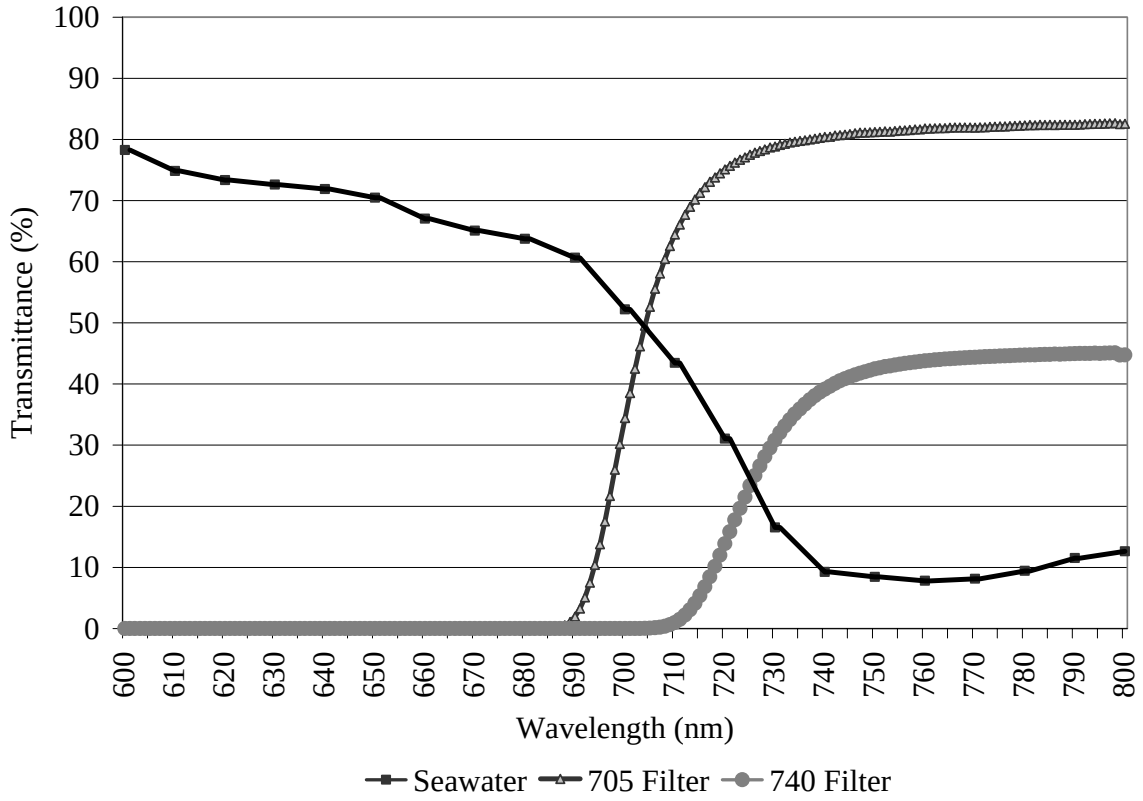

Figure 2. Transmittance spectra for the two filters used in this study, along with a computed transmittance spectrum for pure seawater at a depth of 1 m.

Experiment

The project area for the study was Fort Desoto, Florida (Figure 3). This area was selected because it contains a beach that is sheltered from wave action. This was an important criterion in that wave run-up would have complicated both the photogrammetric shoreline delineation and the field work performed to obtain a reference shoreline with GPS. The small bay shown in Figure 3 contains a variety of bottom types ranging from sandy to vegetated with sea grass.

Two metric aerial cameras were used in Phase 1: a Wild RC30 fitted with the 740 nm filter and an RC10 fitted with the 705 nm filter. To enable simultaneous acquisition with the two filters, both cameras were installed on a NOAA Citation aircraft with dual-camera ports. Because the RC10 was not equipped to be controlled by the flight management software, it was linked to the RC30 to allow simultaneous exposure.

Prior to installing the long wavepass filters, an inter-camera comparison was performed using AGFA 80 panchromatic emulsion. In this comparison, exposure settings were equally bracketed on both cameras after the base exposure was established. The film from the two cameras was then spliced and run through the developer simultaneously. Next, the photography was analyzed by NOAA quality control experts using a GAM digital densitometer to determine the exposure settings that yielded photographs of identical density values in sample areas in the photographs from each camera. This procedure verified that virtually no variations in exposure existed between the cameras systems selected for the project photography.

Figure 3. Study area located at Fort Desoto Park.

Using the dual-camera setup, B&WIR photography of the Fort Desoto project area was then acquired simultaneously with the 705 and 740 nm filters on November 11, 2003. Two strips of six photos were acquired with each camera. To eliminate uncontrolled variables, B&WIR film from the same roll was used on the two cameras. After acquisition, the film from the two cameras was spliced and run through the developer at the same time. Several scan iterations were made from the film using various exposures. The quality control experts visually compared these scans with the original film and selected the scan exposure that most closely matched the film. No dodging was performed during the scanning process.

Concurrent with the airborne data collection, a field survey crew used GPS to survey the land/water interface on the ground. The field crew utilized aircraft radios to communicate with the flight crew so as to coordinate the acquisition of the GPS reference data as precisely as possible with the airborne data acquisition. At the time of each exposure, the field crew placed survey pins in the sand marking the land/water interface at approximately 10 m intervals. Kinematic GPS was then used to survey the land/water interface, stopping briefly at each pin. Static GPS with five-minute occupation times was used to obtain precise positions of the survey pins. The GPS reference station was set up in the project area so that the maximum baseline length was less than 3 km.

Both the kinematic and static GPS were post-processed using differential, dual-frequency carrier-phase combinations with integer ambiguities resolved. The post-processed kinematic GPS was then checked against the static GPS and found to agree to within 10 cm. Next, the GPS land/water interface data were converted to Shapefile format and projected in UTM (NAD83) Zone 17 North. This data set served as a reference against which the land/water interface vectors delineated from the stereo photography could be compared.

A simultaneous bundle adjustment was performed on the four strips of photography using the program ORIMA in SocetSet (BAE Systems, San Diego, California), a softcopy photogrammetry software package. Next, four compilers of varying experience levels delineated the land/water interface from both the 705 nm and 740 nm filter imagery. One of the four compilers had participated in the field data acquisition, but was not permitted to view the processed reference vector. The other three compilers had not participated in the field survey and also had no forehand knowledge of the reference data.

The comparison of the compiled land/water interface vectors with the GPS reference was performed in ArcView 3.2 (ESRI Inc., Redlands, California). The kinematic GPS points were considered "truth" while the compiled vectors were considered "test." A spatial join was performed in ArcView between the truth points and the test vectors. The spatial join calculated the distance between each point at the closest position along the test vector. A land/water polygon was created from each shoreline vector to further classify the vector as landward or seaward of the kinematic points. We defined the distance to be positive when the compiled vector is landward of the GPS points and negative when it is seaward of the GPS points. These distances were summarized by the mean (landward/seaward bias) and Root Mean Square Error (RMSE). Additionally, all between-filter differences were compared using Wilcoxon Signed Rank Tests.

Results

The magnitude of the mean error and the RMSE were smaller for each of the four compilers when the vectors were compiled from the 740 filter imagery than from the 705 filter imagery (Table 1). For all compilers and both filters, the mean errors were negative indicating a seaward bias in the compiled land/water interface vectors (Table 1). The mean error was greater in magnitude for each compiler when using the 705 filter, indicating a larger seaward bias. Considering all compilers together, the mean shoreline error was -1.17 m with the 705 nm filter compared to -0.88 m with the 740 nm filter, and the RMSE was 1.50 m for the 705 nm filter compared to 1.31 m with the 740 nm filter.

The results of the Wilcoxon Signed Rank Test indicate all between filter comparisons were significant at the P = 0.001 level (Table 2). Although the difference between the results from the two filters is statistically significant, it is nevertheless smaller than might be anticipated. One possible reason that the compiled shorelines do not differ more is that, as noted above, the cut-on wavelength for the 740 nm filter used in this study is actually 725 nm.

Shoreline	Mean (m)	RMSE (m)
740- Compiler 1	-0.59	0.94
705- Compiler 1	-0.71	0.97
740- Compiler 2	-1.56	1.94
705- Compiler 2	-1.88	2.51
740- Compiler 3	-0.39	0.92
705- Compiler 3	-0.92	1.05
740- Compiler 4	-0.98	1.45
705- Compiler 4	-1.18	1.46

Table 1. Results for each compiler for each filter based on comparison of the compiled land/water interface against the GPS ground truth. The mean error is negative in all cases, indicating a seaward bias in all photogrammetrically compiled vectors. For all compilers, the magnitude of the mean error and the RMSE were lower using the 740 filter.

Compiler	*Z*	P
1	-6.996	< 0.001
2	-6.468	< 0.001
3	-19.264	< 0.001
4	-9.486	< 0.001

Table 2. Results of the Wilcoxon Signed Rank Test. It is apparent that the two distributions are statistically separable.

As a means of further quantifying differences between the 705 nm and 740 nm filter imagery, we next computed the image intensity gradient across the land/water interface for each set of imagery. To perform this analysis, we first selected sample locations at approximately 5 m spacing along the shoreline in the imagery. We then defined image intensity gradient as a function of a single variable: the distance, *r*, perpendicular to the

land/water interface at each sample location (Equation 2). The image intensity gradient at each sample location is then given by Equation 3.

$$Intensity \{ I(r) \tag{2}$$

$$Gradient \{ \frac{\nabla I}{\nabla r} \Sigma \frac{\times I}{\times r} \tag{3}$$

The next step in computing the image intensity gradient across the land/water interface was to extract two points (landward point and seaward point) along the perpendicular to the land/water interface at each sample location. This was performed manually by a human analyst after overlaying the GPS reference shoreline and photogrammetrically compiled shoreline over the imagery. Once the landward point and seaward point were selected at each sample location, the image intensity gradient across the land/water interface was computed using Equation 3. We compute $\times I$ from the difference in digital numbers (DNs) between the landward and seaward points, and $\times r$ is the distance between the two points.

Table 3 shows the image intensity gradients across the land water interface for both the 705 nm imagery and 740 nm imagery. As indicated by the data in the table, the image intensity gradient across the land/water interface is over 50% greater in the imagery acquired with the 740 nm filter than with the 705 nm filter. This translates to greater contrast at the land water interface and improved capability to delineate the shoreline from tide-coordinated B&WIR photography collected with the 740 nm filter.

Filter	Mean image intensity gradient across land/water interface (DN/m)	Standard deviation of image intensity gradient (DN/m)
705	22.5	10.2
740	34.2	14.7

Table 3: Mean image intensity gradient across the land/water interface and corresponding standard deviation for the imagery collected with each filter.

We next computed the correlation between image intensity gradient across the land/water interface and shoreline error for each of the four compilers (Table 4). Compiler 3 was the most experienced and Compiler 1 had participated in the field GPS acquisition. The correlation between image intensity gradient and shoreline error was low for these two compilers. The correlation is higher for Compiler 2 and higher still for Compiler 4, who had the least shoreline compilation experience. Considered together, the data in Tables 3 and 4 indicate that filter selection is more important with less experienced compilers. The correlation between image intensity gradient across the land/water interface and shoreline error for Compiler 4 is illustrated graphically in Figure 4.

	Compiler 1	Compiler 2	Compiler 3	Compiler 4
r value	-0.368	-0.601	-0.404	-0.681

Table 4. Correlation coefficients between a compiler's shoreline error and the associated image intensity gradient across the land/water interface.

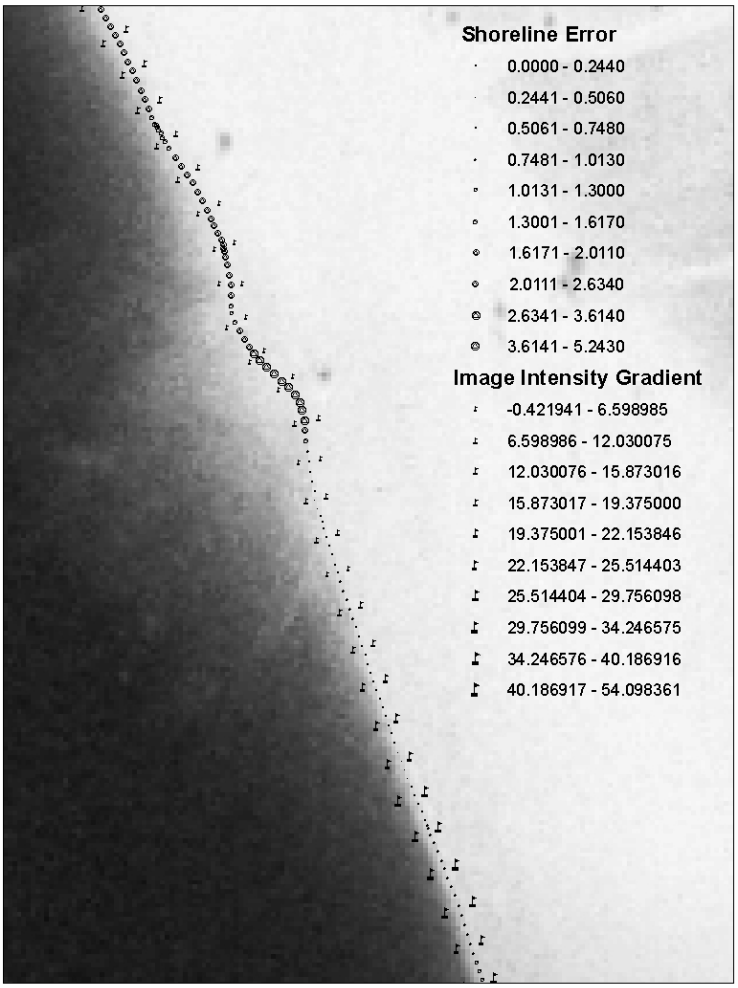

Figure 4. In areas where the intensity gradient across the land/water interface is low, a compiler has a more difficult time delineating the shoreline. The correlation between image intensity gradient across the land/water interface and shoreline error is greatest for less experienced compilers.

PHASE 2

Experiment

The second phase of this study entailed utilizing hyperspectral imagery to simulate film photography with different filters. The advantage of hyperspectral imagery is the capability to analyze greater spectral ranges and compare narrow bandpass channels individually. The data acquisition for Phase 2 was performed using a CASI 2 (Itres, Inc., Calgary, Canada) pushbroom imaging spectrometer installed on the NOAA Citation aircraft. The hyperspectral imagery was acquired from a flying height of 4,500 ft (1,370 m) at a flying speed of approximately 145 kts with a 33 ms integration time. Seventy-two spectral bands were acquired with a bandwidth (full width half maximum) of 8 nm. The data were post-processed by Itres personnel to create georeferenced mosaics with 2.0 by 2.4 m pixels.

Because the airborne data acquisition for Phase 2 was completed four months after the Phase 1 data collection and at a very different stage of tide, the imagery from the two phases could not be inter-compared. Furthermore, it was not possible to use the GPS reference shoreline from Phase 1 in the Phase 2 analysis. Therefore, during the airborne data collection for Phase 2, a field crew collected a new GPS reference land/water interface vector using the procedures previously discussed.

Since reference data existed for only a portion of the project area, the next step was to extract a reference

land/water interface vector that spanned the entire project area and agreed well with the reference data in the area of overlap. Through an iterative testing process using different procedures on different combinations of bands, it was found that the following method produced a land/water interface vector that agreed most closely with the ground-truth GPS reference data: First, a Minimum Noise Fraction (MNF) transformation was run on a subsetted spectral range image spanning 470 to 870 nm. MNF is a two-step principal components transformation used to segregate noise in the data (Van Der Meer, 1999). Upon visual inspection of the MNF image, band 1 was selected for K-means unsupervised classification. Using this algorithm, two output classes were specified to represent land and water. A vector was then auto-extracted at the boundary of these two classes. This process generated a land/water interface vector that spanned the entire study area and agreed closely with the ground-truth data in the area of overlap (Figure 5).

Figure 5. Comparison of K-Means-derived land/water interface (blue) with "ground-truth" GPS data (red).

Next, to simulate B&WIR film with 740 and 705 nm long wavepass filters, the ENVI function *Sum Data Bands* was run on the Desoto Beach reflectance image. The long wavelength limit of the spectral sensitivity region of the B&WIR film used in the first phase of this study is approximately 900 nm. Therefore, to simulate 740 nm and 705 nm filter images, CASI bands were summed to form images that ranged from 742.9 nm to 897.0 nm and from 704.6 nm to 897.0 nm, respectively. After summing the bands, the ENVI K-Means unsupervised classification algorithm was used to output two classes: land and water. A difference image was then created in order to quantify the over-classification of land in the 705 nm filter image as compared to the 740 nm filter image. In Figure 6, the yellow pixels represent water that was misclassified as land in the 705 nm filter image but correctly classified as water in the 740 nm filter image.

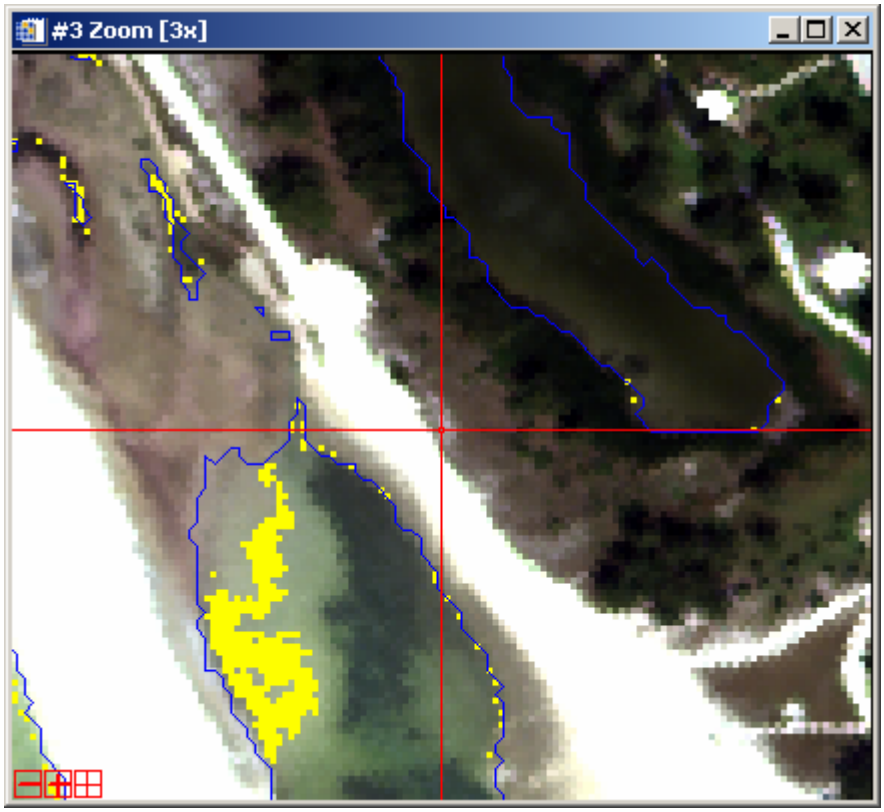

Figure 6. Difference image in which yellow pixels represent water that was misclassified as land in the 705 nm filter image but correctly classified as water in the 740 nm filter image.

Results

As one might expect, the difference in pixel misclassification between the simulated 705 nm imagery and 740 nm imagery seems to be a function of the physical characteristics of the beach. The greatest differences occurred in areas where the beach had a gentle slope with a highly-reflective, sandy bottom. In other areas, the difference between the 740 nm and 705 nm images was negligible. Interestingly, the largest differences in pixel misclassification occurred on the opposite side of the bay from the small beach used in the Phase 1 analysis. Hence, the differences between the shorelines compiled from the two sets of film photography in Phase 1 might have been greater had the study site been enlarged to include the entire bay.

Summing bands to simulate film photography is clearly not the best method of extracting the land/water interface from hyperspectral imagery. However, the benefit in using hyperspectral imagery in this analysis of film-based camera filters is the greater spectral range and the capability to examine narrow bandpass channels individually. Figure 7 shows the CASI bands centered at the following wavelengths: 647, 700, 739, 800, 854, and 900 nm. From the figure, it can be seen that the contrast between land and shallow water continues to improve up to about 800 nm. Beyond 800 nm, very little difference is seen at the land/water interface.

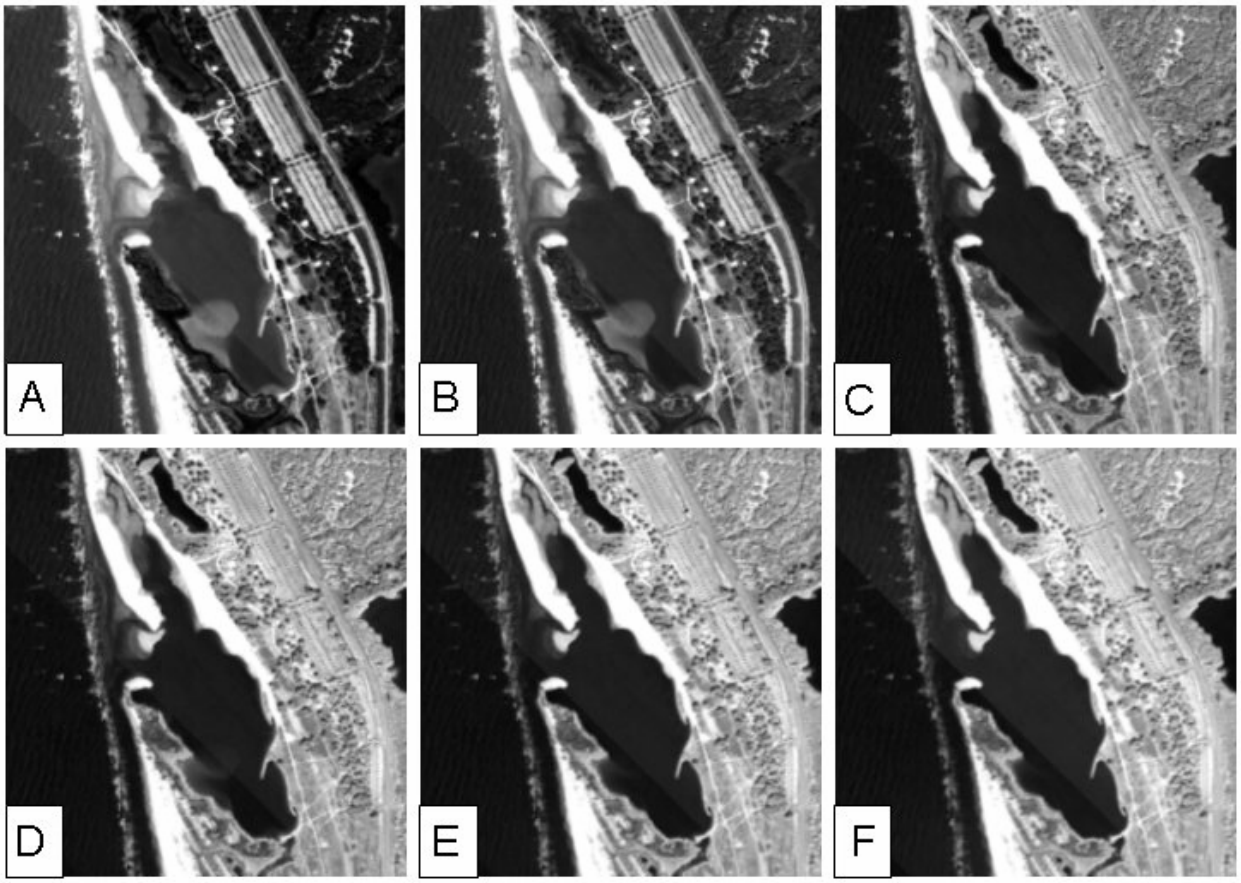

Figure 7. CASI bands centered at the following wavelengths: A) 647 nm, B) 700 nm, C) 739 nm, D) 800 nm, E) 854 nm, and F) 900 nm

CONCLUSIONS

The results of the two phases of this study provide strong indication that filter selection is an important factor in accurate and consistent shoreline delineation from tide-coordinated, B&WIR photography. In Phase 1, the magnitude of the mean error and the RMSE were both larger when delineating the land/water interface from the imagery acquired with the 705 nm filter than with the 740 nm filter. Although the differences were relatively small (on the order of a couple decimeters), the compiled shoreline agreed more closely with the reference shoreline for all four compilers when utilizing the imagery acquired with the 740 nm filter. We speculate that the differences would have been greater had the study site been enlarged to include the opposite side of the small bay and/or if the cut-on for the 740 nm filter used in this study were actually closer to 740 nm.

It was shown that the image intensity gradient across the land/water interface is over 50% greater in the imagery acquired with the 740 nm filter than with the 705 nm filter. The correlation between image intensity gradient and shoreline error appears to be greatest for less experienced compilers. We conclude, therefore, that filter selection is most important with less experienced compilers.

The results of Phase 2 support those of the first phase. Automated classification routines resulted in many more water pixels being misclassified as land in the simulated 705 nm filter imagery than in the simulated 740 nm imagery. We observed that the affects of filter selection are a function of the physical characteristics of the beach. In this study, the greatest differences were seen in areas of shallow water over bright sandy bottom. The differences were smaller in areas of vegetated bottom. However, the spectral properties of aquatic plants vary by location, plant type and season. Future research will involve conducting similar studies in different geographic locations with different beach types and aquatic vegetation. Continued studies will also focus on improved algorithms for

extracting shoreline from hyperspectral imagery, and improvements in information about the coastal environment through fusion of data from multiple sensors.

ACKNOWLEDGEMENTS

The authors are indebted to the following individuals who made significant contributions to this study: Jen Aitken of Optech International, Doug Graham, Danielle Stuby, Ivan Tauler, Bob Clark, Bill Hawken, Jason Woolard, and George Leigh of NOAA, National Geodetic Survey.

REFERENCES

Gates, D.M., H.J. Keegan, J.C. Schleter, and V.R. Weidner (1965). Spectral Properties of Plants. *Applied Optics*, 4:1, pp. 11-20.

Gordon, H.R. (1989). Can the Lambert-Beer law be applied to diffuse attenuation coefficient of ocean water? *Limnology and Oceanography* 34(8), pp.1389-1409.

Graham, D., M. Sault, and J. Bailey (2003). National Ocean Service shoreline—past, present, and future. *Journal of Coastal Research*, SI(38), pp. 14-32.

Itres (2003). *The CASI Manual*. Itres Research Limited, Calgary, Alberta, Canada, 284 p.

Keller, M. (1974). Aerial photography for photogrammetric mapping in the NOS Coastal Mapping Division. National Ocean Survey, Rockville, MD.

Leica (2003). *RC30 Aerial Camera System Technical Reference Manual*. DOC code TRM 507853, Leica Geosystems GIS & Mapping, AG, Switzerland.

Lillesand, T.M., and R.W. Kiefer (2000). *Remote Sensing and Image Interpretation*, Fourth Ed., John Wiley & Sons, Inc., New York, NY.

Sabins, F.F. Jr. (1987). *Remote Sensing Principles and Interpretation*, 2nd Ed., W.H. Freeman and Company, New York, pp. 41-43.

Slater, P.N. (1975). "Photographic Systems for Remote Sensing," in *Manual of Remote Sensing*, R.G. Reeves (Ed.), American Society of Photogrammetry, Falls Church, Virginia, pp. 310-320.

Smith, J.T. Jr. (1978). NOS photographic operations for photobathymetry. Proceedings Coastal Mapping Symposium, American Society of Photogrammetry, August 14-16, Rockville, MD, pp. 67-69.

Smith, R.C., and K.S. Baker (1981). Optical properties of the clearest natural waters (200-800
nm). *Applied Optics* 20:2, pp. 177-184.

Swanson, L.W. (1960). Photogrammetric Surveys for Nautical Charting, Use of Color and Infrared Photography. *Photogrammetric Engineering*, 26:1, pp. 137-141.

Van Der Meer, F. (1999). Iterative Spectral Unmixing (ISU). *International Journal of Remote Sensing*. 20:17, pp.3431-3436

Yost, E., and S. Wenderoth (1968). Coastal water penetration using multispectral photographic techniques. Proceedings of the fifth Symposium on Remote Sensing of Environment, Apr. 16-18, 1968, Ann Arbor, MI.